BRITISH JOURNAL OF HOSPITAL MEDICINE

CASE REPORT

Imaging Features of Primary Clear Cell Carcinoma of the Liver: A Case Series and Literature Review

Lifeng Xu[1], Jingru Dai[2], Guifen Wei[3], Bifeng Zhang[4,*], Ping Zhu[2,*]

[1]Department of Radiology, Tong Xiang First People's Hospital, Tongxiang, Zhejiang, China
[2]Department of Radiology, The Second Affiliated Hospital of Zhejiang Chinese Medical University, Hangzhou, Zhejiang, China
[3]Department of Hepatobiliary Surgery, Tong Xiang First People's Hospital, Tongxiang, Zhejiang, China
[4]Department of Radiology, The Affiliated People's Hospital of Ningbo University, Ningbo, Zhejiang, China
*Correspondence: 13777975725@163.com (Bifeng Zhang); 20194007@zcmu.edu.cn (Ping Zhu)

Abstract

To analyse the computed tomography (CT) and magnetic resonance imaging (MRI) features of primary clear cell carcinoma of the liver (PCCCL), and to provide a diagnostic basis for its identification and differentiation from other lesions. Clinical and imaging data of five patients with surgically and pathologically confirmed PCCCL were retrospectively collected and analysed. All patients underwent non-contrast and dynamic contrast-enhanced CT and MRI scans. On non-contrast CT, all five lesions appeared hypodense, with the lowest CT attenuation values measured in the lesions within the negative range, suggestive of intralesional fat components. On MRI, T1-weighted imaging showed hypointensity in three cases, isointensity in one case, and mild hyperintensity in one case. T2-weighted fat-suppressed sequences revealed heterogeneous—both high and low—signals in four cases and mild hypointensity in one case. Dual-echo sequences demonstrated signal drop on opposed-phase images in all five cases. Diffusion-weighted imaging showed predominantly hypointense signals in one case and heterogeneous hyperintensity (predominantly hyperintense) in four cases. The apparent diffusion coefficient values were preserved in two cases but reduced in three cases. Dynamic contrast-enhanced imaging showed arterial phase enhancement in all five lesions, with washout to hypodense or hypointense patterns in the portal venous and delayed phases. Nodular enhancement was observed in one lesion, prominent intratumoral vessels in one case, and delayed capsular enhancement in two cases. Neither CT nor MRI revealed portal vein tumour thrombus, intrahepatic metastases, lymphadenopathy in the hepatic hilum or retroperitoneum, or ascites. PCCCL is a rare subtype of hepatocellular carcinoma. Identifying its distinct imaging findings, such as peripheral solitary lesions, intratumoral fat, and a high incidence of pseudocapsule formation, may enhance diagnostic accuracy.

Key words: case report; liver; clear cell carcinoma; computed tomography; magnetic resonance imaging; imaging findings

Submitted: 20 July 2025 Revised: 4 September 2025 Accepted: 10 September 2025

How to cite this article:
Xu L, Dai J, Wei G, Zhang B, Zhu P. Imaging Features of Primary Clear Cell Carcinoma of the Liver: A Case Series and Literature Review. Br J Hosp Med. 2025. https://doi.org/10.12968/hmed.2025.0642

Copyright: © 2025 The Author(s).

Introduction

Primary clear cell carcinoma of the liver (PCCCL) represents a rare and distinct pathological subtype of hepatocellular carcinoma. PCCCL is more commonly observed in men over 50 years of age and is frequently associated with hepatitis B or C virus infection, as well as liver cirrhosis. Often without specific clinical symptoms, patients affected by PCCCL are mostly found to suffer from right upper abdominal

pain or liver space-occupying lesions during physical examination (Kothadia et al, 2017).

The tumour cells in PCCCL cases are characterised by a high content of neutral glycogen and lipid components, which render them translucent under microscopic examination. Tumour tissues of PCCCL may contain both immature adipocytes and mature adipose tissue components. PCCCL is classified as a low-grade malignant tumour, usually well-differentiated and encapsulated by a pseudocapsule. This lesion is generally addressed with complete surgical resection, which affords favourable prognosis and survival rates compared to common-type hepatocellular carcinoma (CHCC) (Hu et al, 2024; Wang et al, 2014).

Computed tomography (CT) and magnetic resonance imaging (MRI) are currently the primary imaging modalities for the clinical diagnosis of liver cancer. The imaging characteristics of PCCCL are distinct from those of conventional hepatocellular carcinoma. However, histologically distinguishing intracytoplasmic steatosis (lipid vacuoles) from mature adipose tissue in the interstitium can be challenging, especially in areas where tumour cells are sparsely distributed. It is worth noting that some PCCCL cases containing mature adipocytes may represent a distinct subtype featuring the coexistence of perivascular epithelioid cell tumour (PEComa) family tumours—which have potential for malignancy—with hepatocellular carcinoma, and there is a partial resemblance in immunohistochemical profiles of these two tumour types. Therefore, when both coexist, it is difficult to accurately distinguishing them on both imaging and pathological examination can be extremely challenging.

This study aims to retrospectively analyse the CT and MRI features of five surgically and pathologically confirmed PCCCL cases, with a focus on characterising the presence of fat using chemical shift imaging and correlating these findings with pathologic evidence, to improve the preoperative diagnostic accuracy for this rare tumour.

Case Report

Case Selection

A total of five patients with pathologically confirmed PCCCL were recruited in the Tong Xiang First People's Hospital from May 2017 to May 2024. All of these cases were diagnosed following surgical resection, histopathological examination, and immunohistochemical staining. All specimens were independently reviewed by two experienced pathologists and subsequently confirmed as PCCCL through consensus diagnosis. Specimens with a clear cell component accounting for less than 50% on hematoxylin-eosin (H&E) staining were excluded from the classification of PCCCL, in adherence to the World Health Organisation (WHO) criteria (Nagtegaal et al, 2020). Initial diagnoses for the included cases were further confirmed by means of immunohistochemical staining. The basic information of the five patients, including three males and two females, is shown in Table 1, and the laboratory, pathological examination, surgical and follow-up results are presented in Table 2. Symptoms of upper abdominal pain or bloating were reported by three

Table 1. Baseline characteristics of the included cases.

Case number	Gender	Age (years)	Medical history
Case 1	Male	42	The patient had a history of chronic hepatitis B for more than 30 years. He felt slightly weak recently and lost some weight, but had no abdominal pain.
Case 2	Male	52	He felt a feeling of fullness and discomfort in the upper abdomen for a week without obvious tenderness. Ultrasound suggested a left hepatic mass.
Case 3	Male	77	A liver mass was incidentally detected by ultrasound during physical examination in another hospital, and he reported no obvious discomfort for 3 days.
Case 4	Female	64	She complained of low back pain for 3 days, with persistent dull pain and progressive deterioration, accompanied by nausea and vomiting.
Case 5	Female	69	A liver mass was incidentally detected by ultrasound during physical examination, and she reported no obvious discomfort for 1 day.

patients, while hepatic occupying lesions were incidentally discovered in two cases during physical examination. Manifestations of liver cirrhosis were present in three patients. All lesions in these included cases were solitary primary lesions.

The CARE Checklist has been attached as **Supplementary material** associated with this article.

CT and MRI

All patients underwent both plain scan and contrast-enhanced CT and MRI scans. CT examinations were performed using a Perspective 32-slice spiral CT scanner (Siemens, Erlangen, Germany, lot number: 59788) with patients positioned supine and their arms raised above the head; scanning covered the region from the diaphragmatic dome to the symphysis pubis. Plain scan was performed first, followed by triple-phase contrast-enhanced scanning (arterial, portal venous, and delayed phases). One hundred millilitres of iopromide (Ultravist 370, 370 mg/mL, iodine concentration 370 mg/mL; Bayer Healthcare, Leverkusen, Germany, lot number: KT02J7B) was utilised as the contrast agent, intravenously injected at a rate of 3.5 mL/s, followed by a 20 mL saline flush at an injection rate of 4.0 mL/s. Scanning time was 25–30 s in the arterial phase, 60–70 s in the portal phase, and 3–5 min in the delayed phase. Scan parameters included: detector collimation width 16 mm × 0.75 mm, tube voltage 120 kV, tube current 420 mA, pitch 1.5, and matrix 512 × 512, with images reconstructed at 5 mm slice thickness and 5 mm interval. MRI examinations were performed using a GE Optima 360 1.5T superconducting MRI scanner equipped with a body phased-array coil (GE, Chicago, IL, USA, lot number: 082427140117). The contrast agent was 15 mL of Gd-DOTA (Dotaline; Guerbet, Paris, France, lot number: KT0A2FP) with a dosage of 0.1 mmol/kg, administered intravenously at the rate of 2.5 mL/s. The scanning time was 20–30 s in the arterial phase, 50–60 s in the portal phase, and 3–4 min in the delayed phase.

Table 2. Laboratory, pathological, surgical and follow-up results of the included cases.

Case number	Laboratory examination	Pathological and immunohistochemical examination	Admission date	Treatment method and follow-up outcomes
Case 1	AFP: 117.60 ng/mL CEA: 1.2 ng/mL	Hepatocellular carcinoma: clear cell type. CK7 (+), CK18 (+), AFP (+), Ki-67 (+) 20%	2023-07-13	Segmental hepatectomy and TACE. During the follow-up, there was no recurrence or metastasis.
Case 2	AFP: 56.5 ng/mL CEA: 3.1 ng/mL	Hepatocellular carcinoma: clear cell type. CK7 (+), AFP (+), Ki-67 (+) 10%	2024-03-22	Segmental hepatectomy and TACE. During the follow-up, there was no recurrence or metastasis.
Case 3	AFP: 102.5 ng/mL CEA: 6.2 ng/mL	Hepatocellular carcinoma: clear cell type. β-catenin (+), AFP (+), Ki-67 (+) 13%	2021-04-21	Segmental hepatectomy and TACE. During the follow-up, there was no recurrence or metastasis.
Case 4	AFP: 76.5 ng/mL CEA: 7.5 ng/mL	Hepatocellular carcinoma: clear cell type. AFP (+), CK7 (+), Ki-67 (+) 15%	2017-08-28	Segmental hepatectomy, TACE and chemotherapy. 2018-01-15: Tumour recurrence occurred. 2019-06-30: The tumour exhibited widespread metastasis, and the patient died subsequently.
Case 5	AFP: 27.5 ng/mL CEA: 5.5 ng/mL	Hepatocellular carcinoma: clear cell type. CK8/18 (+), AFP (+), CD34 (+), HEP (+), Ki-67 (+) 46%	2018-04-25	Segmental hepatectomy. 2020-05-20: Tumour recurrence occurred. 2022-04-02: The tumour exhibited widespread metastasis, and the patient died subsequently.

Notes: The normal reference ranges are as follows: AFP, 0–20 ng/mL; CEA, 0–5.0 ng/mL, +: positive.
Abbreviations: AFP, alpha-fetoprotein; CEA, carcinoembryonic antigen; TACE, transcatheter arterial chemoembolization; CK, cytokeratin; Ki-67, Ki-67 antigen; HEP, hepatocyte antigen; CD34, cluster of differentiation 34.

Sequences acquired included: axial breath-hold T1-weighted dual-echo (repetition time [TR] 6.22 ms, echo time [TE] 4.17/2.08 ms), axial respiratory-triggered fat-suppressed T2-weighted spin-echo (TR 7500 ms, TE 87 ms), axial respiratory-triggered diffusion-weighted imaging (B value: 800, TR 12,000 ms, TE 71 ms), coronal breath-hold fast imaging employing steady-state acquisition (FIESTA) (TR 4.05 ms, TE 1.78 ms), breath-hold two-dimensional magnetic resonance cholangiopancreatography (2D MRCP) (TR 6000 ms, TE 800 ms), axial breath-hold liver acquisition with volume acceleration (LAVA) mask scan, axial breath-hold triple-phase dynamic LAVA-enhanced scanning (TR 6.22 ms, TE 3.13 ms), coronal breath-hold LAVA-enhanced scanning (TR 3.26 ms, TE 1.51 ms), and axial breath-hold LAVA delayed-phase enhanced scanning (TR 6.22 ms, TE 3.13 ms).

Imaging Findings

CT findings of the included cases are as follows: (1) On plain scan, all five lesions appeared hypodense. Four lesions demonstrated heterogeneous density, while one appeared homogeneous. The lowest attenuation values within the lesions measured –10 to –35 Hounsfield units (HU), with an overall mean attenuation of 30 HU. The margins were well-defined in all cases. (2) During the arterial phase of contrast-enhanced CT, all five lesions demonstrated heterogeneous enhancement: mild enhancement was observed in four lesions and marked enhancement in one lesion. One lesion contained a nodular enhancing component, and one lesion displayed prominent intratumoral vessels. In the portal venous phase, all lesions appeared relatively hypodense. Delayed capsular enhancement was seen in two lesions. Fig. 1 demonstrates the presence of lipid components within the liver lesion, with nodular enhancement observed on enhanced scanning.

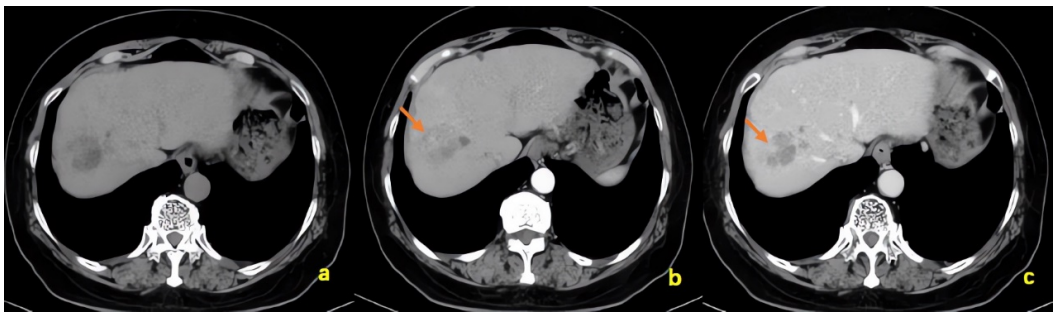

Fig. 1. CT scans for PCCCL in a representative case (male, 42 years old). (a) Plain CT scan showed a low-density lesion in segment VIII of the liver with well-defined margins, and the lowest measured CT attenuation value was –16 HU. (b,c) In the arterial and portal venous phases, the lesion exhibited markedly heterogeneous enhancement, with nodular enhancement shadow (arrows) observed within the lesion. Abbreviations: CT, computed tomography; PCCCL, primary clear cell carcinoma of the liver; HU, Hounsfield units.

MRI findings of the included cases are as follows: (1) On plain scan, three lesions appeared hypointense on T1-weighted imaging (T1WI), one lesion was isointense, and one lesion appeared slightly hyperintense. On fat-suppressed T2-weighted imaging (T2WI), four lesions showed heterogeneous signal intensity with

mixed high and low areas, while one lesion was slightly hypointense. All five lesions demonstrated varying degrees of signal loss on opposed-phase dual-echo gradient-echo imaging. On diffusion-weighted imaging, one lesion was predominantly hypointense, and four lesions exhibited mixed but predominantly hyperintense signals. The apparent diffusion coefficient values were not reduced in two lesions and showed varying degrees of reduction in three lesions. (2) On contrast-enhanced MRI, all five lesions exhibited marked enhancement during the arterial phase. Enhancement diminished in the portal venous and delayed phases, resulting in relative hypointensity. Delayed capsular enhancement was observed in two lesions. Signs of portal hypertension were present in three patients. No definite portal vein tumour thrombus, intrahepatic metastases, and significant lymphadenectasis were detected in the porta hepatis or retroperitoneum, or no ascites formation identified in any of the five cases. Fig. 2 illustrates that the liver lesion exhibits a mixed high- and low-signal intensity on the fat-suppressed sequence of T2WI, a high signal intensity on the T2WI-Iterative Decomposition of water and fat with Echo Asymmetry and Least-squares estimation (T2WI-IDEAL) in-phase sequence, and a significantly reduced signal intensity in the out-of-phase sequence compared to the in-phase sequence. Capsular enhancement is noted at the periphery of the lesion during the delayed phase of contrast-enhanced scanning.

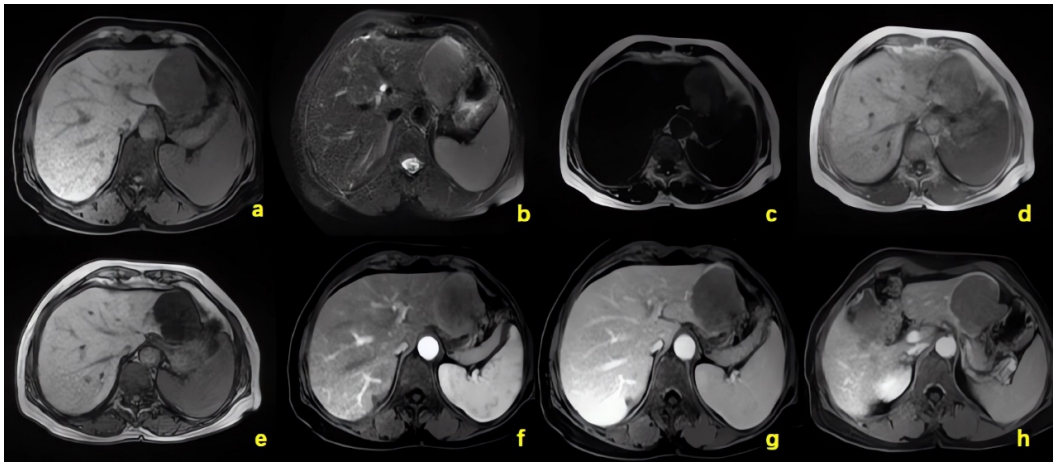

Fig. 2. MRI scans for PCCCL in a representative case (female, 69 years old). (a,b) Space-occupying lesion in liver segments II and III, presenting as low signals on T1-weighted imaging (T1WI) and as mixed high- and low-signals on the fat-suppressed sequence of T2-weighted imaging (T2WI). (c) Lesion with relatively high signal intensity on T2WI-IDEAL in-phase sequence imaging. (d,e) The signal of the lesion in the out-of-phase sequence is significantly weaker than that in the in-phase sequence. (f) Heterogeneous and marked enhancement of the lesion during the arterial phase of the contrast-enhanced scan. (g) A significant reduction in enhancement during the portal venous phase. (h) Capsular enhancement at the periphery during the delayed phase. Abbreviations: MRI, magnetic resonance imaging; PCCCL, primary clear cell carcinoma of the liver; IDEAL, Iterative Decomposition of water and fat with Echo Asymmetry and Least-squares estimation.

Histopathologic Examination

All five patients underwent surgical resection. Gross pathological examination revealed solid tissue with a grayish-white to grayish-yellow cut surface. H&E staining demonstrated that the lesions were predominantly composed of clear cells, characterised by abundant clear cytoplasm and centrally located nuclei exhibiting deep staining and irregular contours (Fig. 3), with intervening fibrovascular septa. Immunohistochemical staining results are as follows: Hep Par1 (hepatocyte marker) was positive in all five cases; cytokeratin 7 (CK7) was positive in one case; CK8/18 was positive in one case; alpha-fetoprotein (AFP) was positive in three cases; Ki-67 antigen (Ki-67) showed 20% positivity in one case; and cluster of differentiation 34 (CD34) was positive in one case. These findings led to a pathological diagnosis of PCCCL in all five patients.

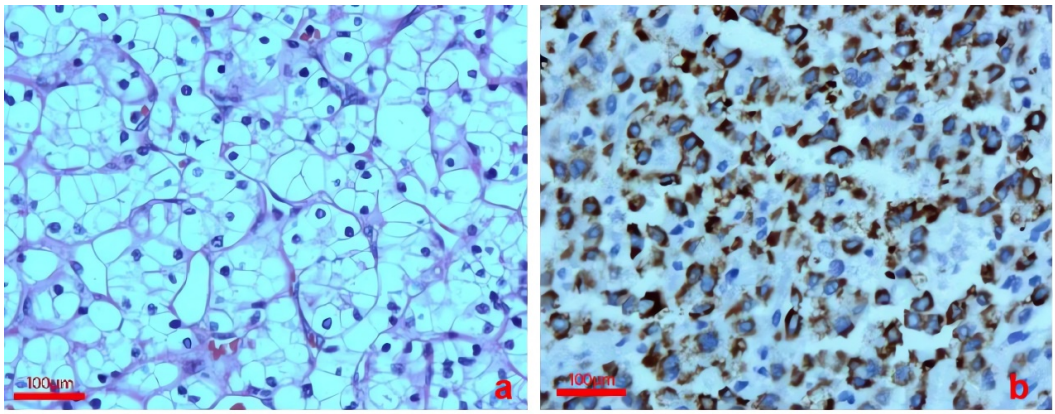

Fig. 3. Histopathological image of a representative PCCCL case. (a) Hematoxylin-eosin staining demonstrates the diffuse distribution of clear cells with abundant cytoplasm, central nuclei, and prominent nuclear staining (magnification ×200). (b) Immunohistochemical analysis reveals positive expression of Hep Par1 (magnification ×200). Abbreviation: PCCCL, primary clear cell carcinoma of the liver.

Discussion

Pathological and Clinical Features of PCCCL

PCCCL is a rare histological subtype of hepatocellular carcinoma (HCC), accounting for approximately 3%–7% of all liver cancers (Zhang et al, 2020). Gross pathological examination reveals that the tumour appears grayish-yellow or grayish-white in colour, with a soft texture. Microscopically, the tumour tissue predominantly consists of clear cells characterised by abundant, translucent cytoplasm. The nuclei exhibit marked irregularity but remain centrally located (Hu et al, 2024). Adjacent hepatocytes often demonstrate lipoid degeneration, indicative of chronic interstitial hepatitis. Although clear cells are commonly observed in most HCC cases, their proportion serves as a critical diagnostic criterion for PCCCL. Before HCC subtypes were clarified in the 2019 fifth edition of the WHO classification of digestive system tumours, there was an inconsistency in the literature regard-

ing the threshold proportion of clear cells required for diagnosing PCCCL. While some scholars proposed that a clear cell proportion exceeding 30% is sufficient for making a PCCCL diagnosis, most pathologists prefer to adopt a criterion of >50%. Tumours with >90% clear cells are extremely rare (Harimoto et al, 2018; Kokubo et al, 2019), which may impact the imaging findings of PCCCL. According to the fifth edition of the WHO classification of digestive system tumours (Nagtegaal et al, 2020), PCCCL can only be diagnosed when clear cells constitute more than 50% of the tumour. A hallmark feature of PCCCL is the glycogen- or lipid-rich cytoplasm of tumour cells, which gives a transparent or vacuolated appearance. Immunohistochemically, PCCCL exhibits translucence of the cytoplasm in most tumour cells, with consistent positivity for Hep Par1 and occasional expression of CK or AFP (Kim et al, 2020; Loy et al, 2022). In this cohort, microscopic analysis confirmed that clear cells accounted for more than 50% of the tumour tissue, with positive expression of Hep Par1 and partial positivity for CK and AFP, fulfilling the pathological diagnostic criteria for PCCCL. Clinically, PCCCL resembles CHCC, with right upper quadrant pain and fatigue as common manifestations, although lesions are often detected incidentally during routine examinations. It is more common in middle-aged and elderly men with a history of hepatitis. Among the cases in this study, all five patients had a history of hepatitis B infection, and three were accompanied by liver cirrhosis. Radical surgical resection remains the primary treatment modality for PCCCL, offering favourable long-term survival outcomes. Wen et al (2021) demonstrated that the survival period of non-surgical PCCCL patients (median overall survival [OS]: 9 months) is shorter than that of surgically treated patients (median OS: 62 months). Tumour size and surgical intervention were identified as independent prognostic factors for OS in PCCCL patients. Patients with small tumours (maximum diameter <1 cm) undergoing surgery achieved superior clinical outcomes. The 1-year, 3-year, and 5-year overall survival rates of PCCCL patients were higher than those of CHCC patients, attributed to a higher degree of cellular differentiation, more intact tumour capsule, lower vascular invasion rate, and reduced incidence of lymph node metastasis (Wen et al, 2021; Xu et al, 2017). Additionally, a study has demonstrated that a higher proportion of clear cells in PCCCL is associated with a higher degree of tumour differentiation and a more favourable prognosis (Park et al, 2019).

Imaging Manifestations and Analysis

Radiologically, PCCCL lesions are commonly solitary and tend to be located at the periphery of the liver. On CT plain scans, these lesions mostly exhibit heterogeneous low-density shadows, with scattered areas of lower density visible within. The measured CT attenuation values of some lesions are negative, indicating the presence of fat components. On MRI T1WI, the lesions predominantly show isointense or slightly hypointense signals, with a few cases demonstrating slightly hyperintense signals. MRI, particularly with chemical shift fat-suppression techniques, is more sensitive than CT in detecting intratumoral fat (Ünal et al, 2016). This is evidenced by T1 signal reduction and mixed hyperintensity and hypointense signals on T2-weighted images, which corresponded to fat-density lesions observed

on CT in four cases. The signal reduction regions were observed in the out-phase of double-echo sequences, confirming the presence of glycogen and lipid components in PCCCL tumour cells. Although the intratumoral fat in PCCCL is an intrinsic component of the tumour cells, the potential influence of patient age on background liver steatosis was considered. However, in our series, the imaging characteristics (e.g., signal loss on opposed-phase MRI) were attributed to the tumour itself, as the surrounding liver parenchyma did not show significant steatotic features.

The pseudocapsule is primarily composed of hepatic sinusoids surrounding the tumour. On dynamic contrast-enhanced scanning, it appears as a peripheral ring-like enhancement, most prominently visualised in the delayed phase. MRI outperforms CT in the imaging of the tumour capsule. It has been reported that cases of PCCCL face a 75% probability of pseudocapsule occurrence (Liu et al, 2021a), whereas 43%–64% of conventional HCC cases feature capsular appearance (fibrous capsule and pseudocapsule) (An et al, 2017; Kim et al, 2018), indicating a higher incidence of pseudocapsule in PCCCL. Pathological examination of PCCCL confirmed the presence of a true fibrous capsule, which is consistent with the "pseudocapsule" observed on imaging.

In contrast-enhanced scans, most PCCCL cases exhibit the classic "fast-in and fast-out" pattern, characterised by marked enhancement in the arterial phase followed by diminished enhancement in the portal venous phase, presenting relatively low density or low signal intensity, similar to the enhancement pattern of conventional HCC (Wang et al, 2014). This similarity often leads to misdiagnosis. However, in a minority of cases, a hypovascular enhancement pattern is observed, characterised by mild enhancement in the arterial phase, which is lower than that of normal liver tissue, and continuous mild-to-moderate enhancement in the portal venous and delayed phases. According to a report, the diversity of imaging manifestations of PCCCL may be related to the proportion of clear cells: the higher the proportion of clear cells, the lower the tumour density on CT, and the more significant the difference in enhancement patterns compared with conventional HCC. Conversely, a lower content of clear cells is associated with a higher degree of resemblance of its enhancement pattern to the "fast-in and fast-out" manifestation of typical HCC (Hu et al, 2024). In this study, all enhanced CT and MRI scans of PCCCL cases conformed to the "fast-in and fast-out" type. One case showed intratumoral vascular signs, and two cases demonstrated delayed capsule enhancement. Studies have reported that the incidence of intratumoral fat signals in PCCCL patients is higher than in HCC patients, while the incidence of intratumoral arterial signs is lower than in HCC patients (Jeon et al, 2023; Liu et al, 2021b). None of the five patients in this study exhibited portal vein tumour thrombus or lymph node metastasis, indicating a high degree of differentiation in PCCCL and a relatively low probability of vascular invasion and lymph node metastasis.

In recent years, the emergence of radiomics and the application of hepatobiliary phase MRI have introduced new approaches to diagnosing PCCCL. Liu et al (2025) compared efficacy of different diagnostic models by enrolling 42 patients with PCCCL and 109 patients with CHCC, who were randomly divided into training and validation sets at a ratio of 2:1. A total of 851 texture features were

extracted to construct the radiomics model and three models were developed: a clinical model, a radiomics fusion model, and a combined model. The area under the curve (AUC) value, sensitivity, specificity and accuracy of each model for PCCCL diagnosis were calculated. The results demonstrated that the combined model achieved the highest performance in both the training set (AUC: 0.940, sensitivity: 1.000, specificity: 0.757, accuracy: 0.820) and the validation set (AUC: 0.868, sensitivity: 0.688, specificity: 0.886, accuracy: 0.824). DeLong test results indicated no statistically significant difference between the clinical model and the radiomics fusion model in either the training set ($p = 0.124$) or the validation set ($p = 0.090$). However, a statistically significant difference was observed between the combined model and the clinical model in both datasets (training set: $p < 0.001$; validation set: $p = 0.004$). The combined model was the clinical model incorporating the radiomics score, which was shown to be an independent factor in distinguishing PCCCL from CHCC. In another study, Song et al (2024) investigated the hepatobiliary phase MRI imaging characteristics of Gadolinium-ethoxybenzyl-diethylenetriamine pentaacetic acid (Gd-EOB-DTPA) in clear cell hepatocellular carcinoma (CCHCC) compared with non-otherwise-specified hepatocellular carcinoma (NOS-HCC). The study analysed clinical, pathological, and MRI data from 42 patients with CCHCC and 84 age-matched patients with NOS-HCC. Univariate and multivariate logistic regression analyses, along with Cox regression analysis, were performed to identify independent diagnostic and prognostic factors for CCHCC. The findings revealed that, compared with NOS-HCC, CCHCC was more likely to exhibit decreased signal intensity on out-of-phase images ($p < 0.001$) and a higher Edmondson tumour grade ($p = 0.001$). Additionally, the lesion-to-muscle ratio (LMR) and lesion-to-liver ratio (LLR) on T1-weighted imaging before contrast enhancement (pre-T1WI) ($p = 0.001$ and $p = 0.003$, respectively) and on hepatobiliary phase images ($p = 0.007$ and $p = 0.048$, respectively) were significantly higher in CCHCC than in NOS-HCC. The AUC values for fat content, LLR on pre-T1WI, and their combination in predicting CCHCC were 0.678, 0.666, and 0.750, respectively. Multivariate Cox regression analysis confirmed that tumour size greater than 2 cm and capsule enhancement were independent prognostic indicators for both disease-free survival and overall survival in patients with CCHCC. These findings suggest that fat content on pre-T1WI and hepatobiliary phase images, along with adjusted lesion signal intensity, can serve as effective differentiating indicators between CCHCC and NOS-HCC.

Differential Diagnosis

Due to the variable appearance of PCCCL on dynamic contrast-enhanced imaging, it must be differentiated primarily from CHCC, hepatic angiomyolipoma (HAL), hepatic cavernous hemangioma, and metastatic clear cell carcinoma of the liver, among other lesions. Generally, CHCC features large vessel invasion, elevated serum AFP levels, and large tumour size, with the longest diameter usually exceeding 5.0 cm. Enhanced scanning of CHCC demonstrates marked enhancement in the non-marginal arterial phase and rapid washout in the portal venous and delayed phases, presenting a characteristic "fast-in and fast-out" enhancement pattern (Auer

et al, 2023; Cannella et al, 2021; Vande Lune et al, 2018), which is hardly distinguishable from the "fast-in and fast-out" enhancement pattern of PCCCL. However, PCCCL tends to form pseudocapsules and contains a relatively high amount of lipid components—characteristics that are valuable for differential diagnosis. In cases where PCCCL lesions have abundant fat and exhibit "slow-in and slow-out" enhancement patterns on imaging, careful differentiation from HAL is required. The fat in HAL is predominantly composed of mature adipocytes, exhibiting a lower CT attenuation value, generally less than –50 HU. Moreover, HAL rarely presents with a capsule and is not typically associated with a history of chronic liver disease. Contrast-enhanced imaging typically shows continuous enhancement of the HAL lesion, often accompanied by punctate or vascular structures within the tumour. Especially, the presence of enhanced vascular shadows in the fat component is a characteristic sign of HAL (Yang et al, 2023). On the other hand, hepatic hemangiomas typically present as uniformly isodense or slightly hypodense on CT scans, without a pseudocapsule. Enhanced scanning shows nodular enhancement at the edge of the lesion in the arterial phase and progressive centripetal filling in the portal venous and delayed phases (Liu et al, 2020), whereas PCCCL enhancement usually does not demonstrate a filling trend. Under microscopic examination, PCCCL and metastatic clear cell carcinoma of the liver originating from the kidneys, ovaries, or adrenal glands exhibit similar cell morphology, structure, and arrangement, making differentiation difficult. In light of the challenges in differential diagnosis, understanding the patient's primary tumour history would aid in effectively achieving a clear diagnosis for PCCCL. Other than histopathological and imaging approaches, immunohistochemical analysis of the hepatogenic immune marker Hep Par1 offers an efficient diagnostic strategy due to its specificity for PCCCL.

Limitations

This study has several limitations that must be acknowledged. Firstly, a primary limitation of this case series is its small sample size, comprising only five cases. This limited cohort may affect the generalizability of findings, such as estimates of the incidence of pseudocapsule or intratumoral fat. Thus, future multicentre studies with larger cohorts are warranted to validate our observations. Second, although the CT and MRI protocols were generally standard, variations in their applications across patients due to the extended time span of data collection may have impacted the consistency of quantitative measurements. Finally, the potential of more advanced imaging techniques, such as hepatobiliary-phase imaging with gadoxetic acid or radiomics analysis, was not explored in this cohort due to its retrospective design. Future prospective, multi-centre studies with larger samples are essential to validate our findings and further elucidate the full imaging spectrum of PCCCL.

Conclusion

In conclusion, despite its rarity, PCCCL should be considered in the differential diagnosis of solitary peripheral liver lesions exhibiting intratumoral fat and a pseudocapsule, especially those showing a "fast-in and fast-out" enhancement pat-

tern. Identifying these distinctive imaging features of PCCCL, particularly on MRI with chemical shift sequences, is crucial for making an accurate diagnosis and guiding clinical management, as this approach can lead to a more favourable prognosis compared to CHCC.

Learning Points

- Primary clear cell carcinoma of the liver (PCCCL) is a rare malignancy diagnosed only when the clear cell component exceeds 50% of the tumour, characterised by cells with abundant lipid content.
- Distinctive CT and MRI features of PCCCL include solitary peripheral lesions, intratumoral fat, and a pseudocapsule, which are key diagnostic indicators.
- Although current CT and MRI provide valuable diagnostic information, this study is limited by its small sample size, underscoring the need for larger cohorts and advanced imaging techniques to enhance diagnostic accuracy.

Availability of Data and Materials

All data included in this study are available from the first author upon reasonable request.

Author Contributions

LFX and JRD were responsible for the data curation and drafting of the original manuscript. GFW and BFZ performed the investigation and formal analysis. BFZ and PZ provided the resources and validation, and LFX and PZ contributed to the conceptualisation and project administration. All authors contributed to the important editorial changes in the manuscript. All authors read and approved the final manuscript. All authors have participated sufficiently in the work and agreed to be accountable for all aspects of the work.

Ethics Approval and Consent to Participate

This study was approved by the Ethics Committee of Tong Xiang First People's Hospital (Zhejiang, China) (Ethics approval number: 2025-027-01) and conducted in accordance with the Declaration of Helsinki. As this is a retrospective case report without identifiable patient information, the Ethics Committee of Tong Xiang First People's Hospital granted an exemption from patient-informed consent.

Acknowledgement

Not applicable.

Funding

This research was supported by the Zhejiang Provincial Medical and Health Science and Technology Project (Fund number: 2025KY1643).

Conflict of Interest

The authors declare no conflict of interest.

Supplementary Material

Supplementary material associated with this article can be found, in the online version, at https://www.magonlinelibrary.com/doi/suppl/10.12968/hmed.2025.0642.

References

An C, Rhee H, Han K, Choi JY, Park YN, Park MS, et al. Added value of smooth hypointense rim in the hepatobiliary phase of gadoxetic acid-enhanced MRI in identifying tumour capsule and diagnosing hepatocellular carcinoma. European Radiology. 2017; 27: 2610–2618. https://doi.org/10.1007/s00330-016-4634-6

Auer TA, Halskov S, Fehrenbach U, Nevermann NF, Pelzer U, Mohr R, et al. Gd-EOB MRI for HCC subtype differentiation in a western population according to the 5th edition of the World Health Organization classification. European Radiology. 2023; 33: 6902–6915. https://doi.org/10.1007/s00330-023-09669-y

Cannella R, Dioguardi Burgio M, Beaufrère A, Trapani L, Paradis V, Hobeika C, et al. Imaging features of histological subtypes of hepatocellular carcinoma: Implication for LI-RADS. JHEP Reports: Innovation in Hepatology. 2021; 3: 100380. https://doi.org/10.1016/j.jhepr.2021.100380

Harimoto N, Hagiwara K, Yamanaka T, Ishii N, Igarashi T, Watanabe A, et al. Fairly rare clear cell adenocarcinoma mimicking liver cancer: a case report. Surgical Case Reports. 2018; 4: 97. https://doi.org/10.1186/s40792-018-0500-x

Hu X, Li X, Zhao W, Cai J, Wang P. Multimodal imaging findings of primary liver clear cell carcinoma: a case presentation. Frontiers in Medicine. 2024; 11: 1408967. https://doi.org/10.3389/fmed.2024.1408967

Jeon J, Park J, Lee E, Han J, Kim D, Kim D, et al. Huge Primary Clear Cell Hepatocellular Carcinoma: a Case Report and Review of Radiologic Findings. Current Medical Imaging. 2023. https://doi.org/10.2174/1573405620666230522144730 (online ahead of print)

Kim B, Lee JH, Kim JK, Kim HJ, Kim YB, Lee D. The capsule appearance of hepatocellular carcinoma in gadoxetic acid-enhanced MR imaging: Correlation with pathology and dynamic CT. Medicine. 2018; 97: e11142. https://doi.org/10.1097/MD.0000000000011142

Kim H, Jang M, Park YN. Histopathological Variants of Hepatocellular Carcinomas: an Update According to the 5th Edition of the WHO Classification of Digestive System Tumors. Journal of Liver Cancer. 2020; 20: 17–24. https://doi.org/10.17998/jlc.20.1.17

Kokubo R, Saito K, Shirota N, Wakabayashi Y, Tsuchida A, Nagai T, et al. A case of primary clear cell hepatocellular carcinoma comprised mostly of clear cells. Radiology Case Reports. 2019; 14: 1377–1381. https://doi.org/10.1016/j.radcr.2019.08.021

Kothadia JP, Kaur N, Arju R, Dakhel M, Giashuddin S. Primary Clear Cell Carcinoma of the Non-cirrhotic Liver Presenting as an Acute Abdomen: a Case Report and Review of the Literature. Journal of Gastrointestinal Cancer. 2017; 48: 211–216. https://doi.org/10.1007/s12029-016-9831-7

Liu B, Chen F, Zhang YY, Zhu HF, Li HJ. The value of radiomics in the diagnosis of primary clear cell carcinoma of the liver. Radiologic Practice. 2025; 40: 24–28. (In Chinese)

Liu B, Sun J, Chen F, Li HJ. Accurate Diagnosis of Comprehensive Clinical Imaging Model in Clear Cell Hepatocellular Carcinoma. Chinese Journal of Medical Imaging. 2021a; 29: 897–901. (In Chinese)

Liu B, Yang X, Chen F, Sun J, Li HJ. The value of magnetic resonance imaging in the diagnosis of clear cell hepatocellular carcinoma. Chinese Journal of Magnetic Resonance Imaging. 2021b; 12: 21–24. (In Chinese)

Liu Z, Yi L, Chen J, Li R, Liang K, Chen X, et al. Comparison of the clinical and MRI features of patients with hepatic hemangioma, epithelioid hemangioendothelioma, or angiosarcoma. BMC Medical Imaging. 2020; 20: 71. https://doi.org/10.1186/s12880-020-00465-4

Loy LM, Low HM, Choi JY, Rhee H, Wong CF, Tan CH. Variant Hepatocellular Carcinoma Subtypes According to the 2019 WHO Classification: An Imaging-Focused Review. AJR. American Journal of Roentgenology. 2022; 219: 212–223. https://doi.org/10.2214/AJR.21.26982

Nagtegaal ID, Odze RD, Klimstra D, Paradis V, Rugge M, Schirmacher P, et al. The 2019 WHO classification of tumours of the digestive system. Histopathology. 2020; 76: 182–188. https://doi.org/10.1111/his.13975

Park BV, Gaba RC, Huang YH, Chen YF, Guzman G, Lokken RP. Histology of Hepatocellular Carcinoma: Association with Clinical Features, Radiological Findings, and Locoregional Therapy Outcomes. Journal of Clinical Imaging Science. 2019; 9: 52. https://doi.org/10.25259/JCIS_111_2019

Song M, Tao Y, He K, Du M, Guo L, Hu C, et al. Clear cell hepatocellular carcinoma: Gd-EOB-DTPA-enhanced MR imaging features and prognosis. Abdominal Radiology. 2024; 49: 2606–2621. https://doi.org/10.1007/s00261-024-04263-2

Ünal E, Karaosmanoğlu AD, Akata D, Özmen MN, Karçaaltıncaba M. Invisible fat on CT: making it visible by MRI. Diagnostic and Interventional Radiology. 2016; 22: 133–140. https://doi.org/10.5152/dir.2015.15286

Vande Lune P, Abdel Aal AK, Klimkowski S, Zarzour JG, Gunn AJ. Hepatocellular Carcinoma: Diagnosis, Treatment Algorithms, and Imaging Appearance after Transarterial Chemoembolization. Journal of Clinical and Translational Hepatology. 2018; 6: 175–188. https://doi.org/10.14218/JCTH.2017.00045

Wang H, Tan B, Zhao B, Gong G, Xu Z. CT findings of primary clear cell carcinoma of liver: with analysis of 19 cases and review of the literature. Abdominal Imaging. 2014; 39: 736–743. https://doi.org/10.1007/s00261-014-0104-2

Wen J, Yao X, Xue L, Aili A, Wang J. Predictors and survival of primary clear cell carcinoma of liver: a population-based study of an uncommon primary liver tumor. Translational Cancer Research. 2021; 10: 3326–3344. https://doi.org/10.21037/tcr-21-9

Xu W, Ge P, Liao W, Ren J, Yang H, Xu H, et al. Edmondson grade predicts survival of patients with primary clear cell carcinoma of liver after curative resection: A retrospective study with long-term follow-up. Asia-Pacific Journal of Clinical Oncology. 2017; 13: e312–e320. https://doi.org/10.1111/ajco.12494

Yang W, Sun Q, Shang M, Li S, Hu X, Hu X. Multimodal imaging study of hepatic perivascular epithelioid cell tumors: a case report. Frontiers in Medicine. 2023; 10: 1322048. https://doi.org/10.3389/fmed.2023.1322048

Zhang Z, Xie H, Chen P, Cao P. Development and Identification of a Nomogram Prognostic Model for Patients with Primary Clear Cell Carcinoma of the Liver. Medical Science Monitor. 2020; 26: e919789. https://doi.org/10.12659/MSM.919789